Journal of Power Sources 198 (2012) 158–163

Contents lists available at SciVerse ScienceDirect

Journal of Power Sources

journal homepage: www.elsevier.com/locate/jpowsour

The fabrication of high-aspect-ratio micro-flow channels on metallic bipolar plates using die-sinking micro-electrical discharge machining

Jung-Chung Hung [a], Dyi-Huey Chang [b,*], Yin Chuang [c]

[a] Department of Mechanical Engineering, National Chin-Yi University of Technology, Taiping City, Taichung 411, Taiwan
[b] Department of Environmental Engineering and Management, Chaoyang University of Technology, Wufeng District, Taichung 413, Taiwan
[c] Mold & Precision Machining Technology Section, MIRDC, Taiwan

ARTICLE INFO

Article history:
Received 26 July 2011
Received in revised form
20 September 2011
Accepted 21 September 2011
Available online 29 September 2011

Keywords:
Die-sinking micro-electrical discharge machining
Fuel cells
Metallic bipolar plates
Micro-flow channels

ABSTRACT

This study explores the feasibility of using a relatively rapid technique, die-sinking micro-electrical discharge machining, to fabricate miniature metallic bipolar plates. The flow field is a three-pass serpentine structure, of which both the rib and channel widths are 500 μm and the channel depth is 600 μm (aspect ratio = 1.2) in a reaction area of 20 mm × 20 mm. The material-removal rate of the proposed method can reach up to 7.2 mm^3 min^{-1}. However, a high material-removal rate also increases the surface roughness of flow channels. In single-cell tests, the peak power densities are 674 mW cm^{-2} and 647 mW cm^{-2} for flow channels with a surface roughness of 0.715 μm Ra and 0.994 μm Ra, respectively. Though the increase in surface roughness lowers cell performance, the effect is not statistically significant.

1. Introduction

Proton exchange membrane fuel cells (PEMFCs) have become the focus of energy conversion techniques due to their remarkable features, such as compactness, quiet operation, high power density, and lack of emissions. Since the rapid development of mobile computer, consumer, and communication (3C) applications, and because of the increasing demand for green energy, fuel cells have been considered promising alternatives for lithium-ion batteries. Several high-tech companies even released concept portable products featuring fuel cells. However, the problem of their bulky size must be resolved before fuel cells can be widely accepted in the market.

A typical PEMFC is composed of a proton exchange membrane (PEM), gas diffusion layers (GDL), and bipolar plates. Among them, the bipolar plates comprise almost 60–80% of the weight and 50% of the volume [1–3] and are, therefore, crucial to minimizing fuel cells. Both the materials and fabricating methods must be considered to construct a light, thin bipolar plate. Graphite bipolar plates have been adopted in traditional fuel cell technologies, but their brittleness causes difficulty in precision machining, especially at micro scales. Silicon-based and metallic bipolar plates were, therefore, developed as alternatives to graphite bipolar plates. The fabrications of silicon-based bipolar plates are primarily based on micro-electromechanical systems (MEMS) [4–7]. Though such technology can fabricate fine and complicated flow fields in miniature bipolar plates, the performance of silicon-based fuel cells is not appealing. The poor performance is primarily due to the significantly low electrical conductivity of silicon-based bipolar plates (0.5 S cm^{-1}) compared to that of metallic bipolar plates (5000 S cm^{-1}). Yu et al. [8] applied the dry etching process to silicon wafers to create flow channels with a depth of 200 μm. Metal sputtering was applied to increase electrical conductivity. The cell with the plates of Cu sputtering yielded the best result with a peak power density of 194.3 mW cm^{-2}. Park and Madou [9] applied the carbon-MEMS process to fabricate graphite bipolar plates. The polymer Cirlex® sheets were applied to prepare the micro-flow design through MEMS, and were then carbonized using furnace heat. The peak power density determined through cell tests was relatively high (773 mW cm^{-2}). Though this procedure bypasses the difficulties of directly machining flow channels on graphite bipolar plates, the problem of brittleness while assembling and using fuel cells remains.

In contrast, metallic bipolar plates provide high mechanical strength and can be formed into thin sheets with a thickness ranging from 100 to 500 μm [10–13], and thus have significant potential in the fabrication of miniature fuel cells. Lee et al. [14–16] used SS304 stainless steel as a substrate to form a channel mold via the Lithography Galvanic Abformung (LIGA) process. Ni was

* Corresponding author. Tel.: +886 42 23323000x4530; fax: +886 42 23742365.
E-mail addresses: changdh@cyut.edu.tw, changdh45220@yahoo.com.tw (D.-H. Chang).

0378-7753/$ – see front matter © 2011 Elsevier B.V. All rights reserved.
doi:10.1016/j.jpowsour.2011.09.065

then electroformed into the mold, becoming a metallic bipolar plate. The average peak power density during various cell tests was 195 mW cm^{-2}. However, due to the high costs of both the equipment and the consumables required, the LIGA process is economically inefficient. Furthermore, the complicated photochemical procedures result in variances in the channel sizes and shapes, which consequently limit fuel distribution.

Micro-electrical discharge machining (micro-EDM) is a novel fabrication method for machining micro-structures and components. The maximum aspect ratios of this process associated with various tool pieces range from 10 to 100, and the minimum feature size ranges from 3 to 30 μm [17]. In our previous research [18], micro-EDM milling was used to create miniature SUS316L bipolar plates. During the single-cell tests, the peak power density achieved 723.5 mW cm^{-2}, and the volumetric power density is estimated to be approximately 315 mW cm^{-3}, demonstrating the feasibility of directly machining high-aspect-ratio flow channels on miniature SUS316L bipolar plates. However, micro-EDM milling is a point-processing technique that is time consuming and labor intensive. A relatively rapid process is required if repeated tests for various flow structures or mass production is desired. The primary purpose of this study is to explore the feasibility of using an area-processing technique—die-sinking micro-EDM—for fabricating high-aspect-ratio micro-flow channels. Additionally, because the increase in the processing rate also increased the surface roughness of flow channels, the intricate relationships between the material-removal rate, peak discharging current, surface roughness, and cell performance will be explored and discussed in this study.

2. Design and production of metallic bipolar plates

2.1. Materials and design

The materials for metallic bipolar plates should be carefully selected. Some metals, such as Cu, may be sufficient electrical conductors but they are easily corroded. Using easily-corroded metal lowers the performance and shortens the life of fuel cells. In this study, stainless steel SUS316L was chosen as the plate material. Because SUS316L contains molybdenum, it demonstrates excellent heat and corrosion resistance. To prepare the bipolar plate, a 2 mm-thick SUS316L plate was cut into a 50 mm × 50 mm area using a wire machine. For unipolar plates, a plate with only 1 mm in thickness is required.

Regarding the flow structure, previous studies [19,20] claimed that the serpentine flow field has excellent drainage characteristics and cell performance. However, single-pass serpentine tends to cause polarization problems due to excessive channel length; while excessive passes tend to result in uneven fuel distribution. Therefore, the three-pass serpentine with six U-turns was adopted as the flow design. Fig. 1 shows the designed flow field, of which both the channel rib and widths are 500 μm, and the channel depth is 600 μm (aspect ratio = 1.2) in a 20 mm × 20 mm reaction area.

2.2. Die-sinking micro-EDM

2.2.1. The principle

Micro-EDM is a thermal process that uses electrical discharges to erode electrically conductive materials. During the process, material is removed through a rapid series of pulses from both the work and tool piece electrodes. A constant supply of dielectric liquid insulates the two electrodes within a small gap and transports the debris. Because the tool and work piece do not contact each other, adverse effects from mechanical force and vibrations are minimized.

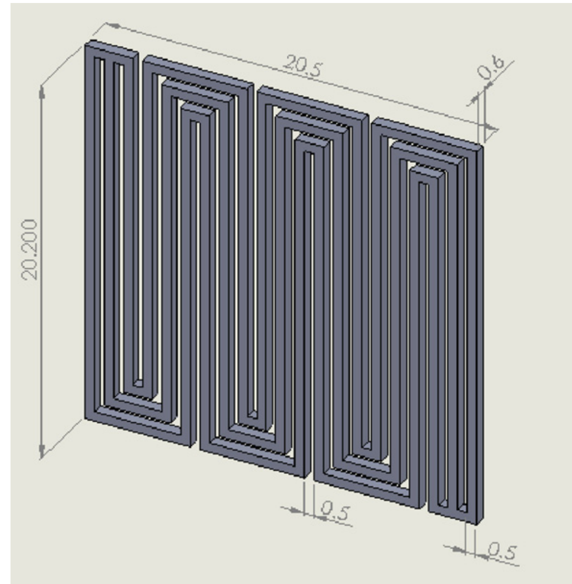

Fig. 1. Schematic representation of the flow design (unit: mm).

The primary difference between the micro-EDM milling applied in our previous research [18] and the proposed die-sinking micro-EDM is in the tool piece electrode, shown in Fig. 2(a) and (b), respectively, as an operational concept. The tool piece electrode of micro-EDM milling was a micro-tungsten rod, sharpened to the designed diameters using wire electrical discharge grinding (WEDG). The work piece electrode, specifically the plain metallic plate, was scanned by the tool piece electrode repeatedly along the paths until reaching the preferred depth. This process is a point-discharging technique and the material-removal rate is relatively slow. In contrast, die-sinking micro-EDM is an area-processing technique, in which a cubic electrode is used and the processing path is a single direction. In other words, the flow field is formed in one-step, which tremendously increases the material-removal rate.

2.2.2. Preparation of tool piece electrode

The tool piece electrode for die-sinking micro-EDM was manufactured using micro-high speed milling (micro-HSM), as shown in Fig. 3(a). A micro-end mill comprised of tungsten carbide with a diameter of 600 μm and a 30° helix angle was applied to form the channels. When using a mill with such a small diameter, an extremely high rotational speed is required to increase the processing rate. This experiment applied a high precision 4-axis CNC micro-HSM center with a maximum rotational speed of 60,000 rpm. A laser interferometer was used to calibrate the accuracy of processing. Meanwhile, the cutting depth and feeding speed must be carefully controlled to avoid breaking the micro-end mills and chipping the work piece.

The optimal operating parameters and the specifications for the electrode are summarized in Table 1. Chrome copper was selected as the electrode material because of its low cost and suitability for sharpening, and its high electrical conductivity. The flow field was sketched by 3D CAD and transformed into processing path through computer-aided manufacturing (CAM). The finished electrode is shown in Fig. 3(b). During the process of die-sinking micro-EDM, the tool piece electrode can be regarded as a complementary mold for flow channels. That is, the ribs in the mold form the channels in the bipolar plate, and vice versa. The channel and rib widths of the tool piece electrode were 600 μm and 400 μm, respectively. Considering the surplus discharge during the EDM process, the

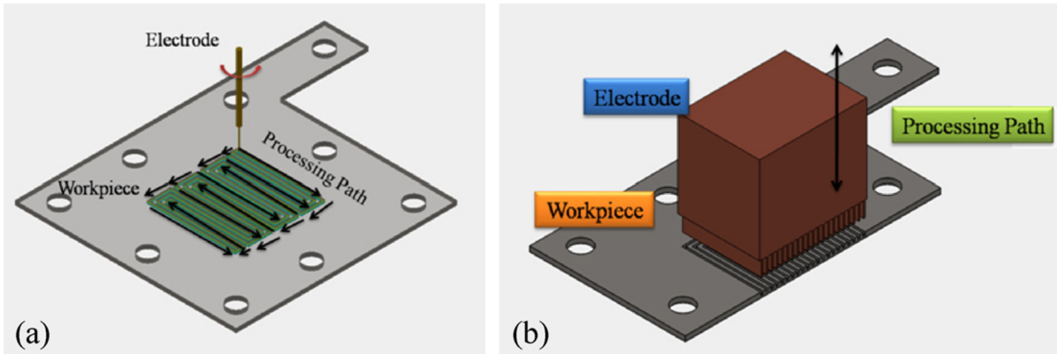

Fig. 2. The tool piece electrodes and processing paths for (a) micro-EDM milling and (b) die-sinking micro-EDM.

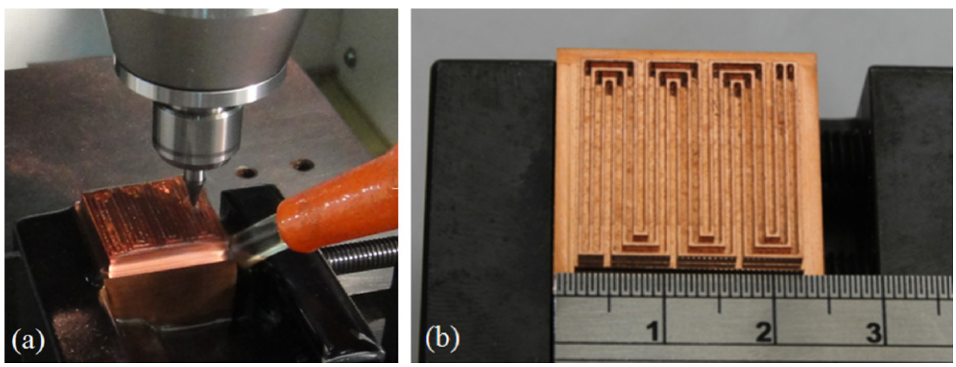

Fig. 3. (a) Preparation of the tool piece electrode for die-sinking micro-EDM and (b) the ready-to-use tool piece electrode.

rib width of the tool piece electrode was 400 μm instead of the designed 500 μm of the bipolar plate. In addition, a relatively deep channel depth (2000 μm) was created because the ribs of the electrode will be consumed during the EDM process.

2.2.3. Fabricating the bipolar plates

The equipment for die-sinking micro-EDM was a high precision 4-axis CNC micro-EDM. The working table was made of granite, and its maximum machining range was 250 mm (X) × 250 mm (Y) × 150 mm (Z). Every axis was driven by motor actuators guided by air bearings in fine-resolution displacement, which enables precision in the sub-micron scale. The tool piece electrode prepared by micro-HSM was installed in the micro-EDM system to process the metallic bipolar plates, as shown in Fig. 4.

The experimental parameters are summarized in Table 2. Kerosene was used as the dielectric because of its low conductivity (0.0017 μS cm^{-1}). Because die-sinking micro-EDM is an area-processing technique, it requires greater electrical energy than other micro-EDM processes. The material-removal rate primarily depends on the peak discharging current, with minor influences from pulse duration and pulse-off time. With a short pulse duration and long pulse-off time, electrical discharge occurs while power density continues to increase, decreasing the electrical discharge energy and amount of material removed. With a longer pulse duration and short pulse-off time, the current density energy is lower but the discharge energy may be insufficient to remove large amounts of material. After several trials, the 160 μs pulse duration and 200 μs pulse-off time were found to provide the optimum balance between the material-removal rate and available energy. Additionally, the raised peak current increased material removal

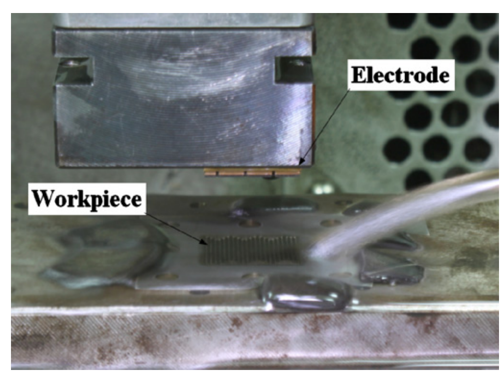

Fig. 4. Processing of metallic bipolar plates.

Table 1
Summary of the micro-HSM process.

Tool	
Micro-end mill	Ø600 μm tungsten carbide micro-end mill
Rotational speed	18,000 rpm
Feeding speed	150 mm min^{-1}
Cutting depth	100 μm
Work piece	
Material	Chrome copper
Channel width	600 μm
Rib width	400 μm
Channel depth	2000 μm

Table 2
Electrical discharge parameters.

Tool piece electrodes	Chrome copper
EDM dielectric	Kerosene
Peak discharging current (A)	1.5, 3, 5, 6
Pulse duration (μs)	160
Pulse-off time (μs)	200
Open voltage (V)	120
Gap voltage (V)	50

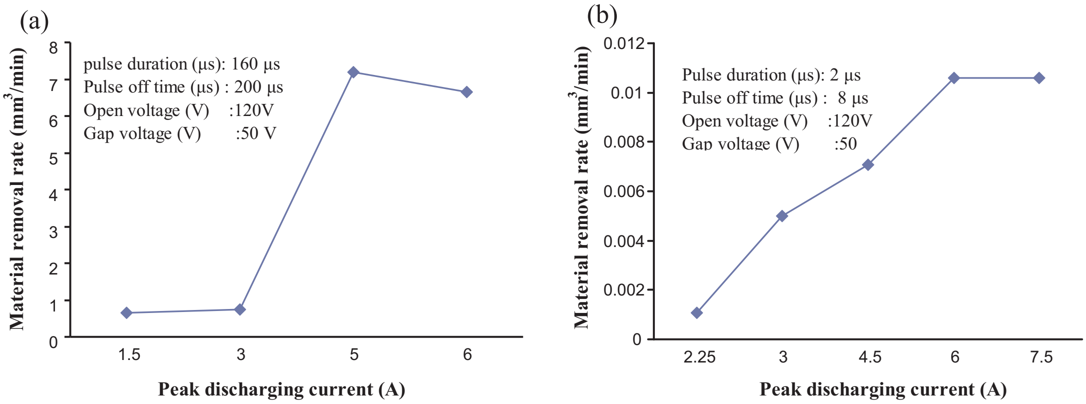

Fig. 5. The relationship between the material-removal rate and peak discharging current for (a) die-sinking micro-EDM and (b) micro-EDM milling.

rate and also enhanced the surface roughness of flow channels. The increase in surface roughness might limit fuel distribution, water drainage, and lower cell performance. The relationships between the material-removal rate, peak discharging current, surface roughness, and cell performance will be explored and discussed in the next section.

3. Results and discussions

3.1. Material-removal rate, peak discharging current, and surface roughness

Fig. 5(a) shows the material-removal rates under various peak discharging currents. For comparison, a similar plot for micro-EDM milling is shown in Fig. 5(b). In Fig. 5(a), the material-removal rates rise in correlation to the increasing peak discharging current; the highest value occurs at 5 A and is 7.2 $mm^3\,min^{-1}$. The material-removal rates decline when the peak discharging current is larger than 5 A. The reason is that the removal of excessive metal debris influences the electrical conductivity of the dielectric, causing an irregular electric discharge. Nevertheless, the maximum material-removal rate was approximately 650-fold higher than the rate using micro-EDM milling (0.0106 $mm^3\,min^{-1}$), as shown in Fig. 5(b).

Fig. 6 shows the impact of the peak discharging current on the surface roughness. The minimum surface roughness is 0.715 µm Ra at 1.5 A and the maximum surface roughness is 0.994 µm Ra at 6 A. Photos of surface roughness created by various peak discharging currents are shown in Fig. 7. A lower discharging current produces smaller craters, lessening surface roughness; while a larger current enhances the impulse on the surface, thus increasing roughness.

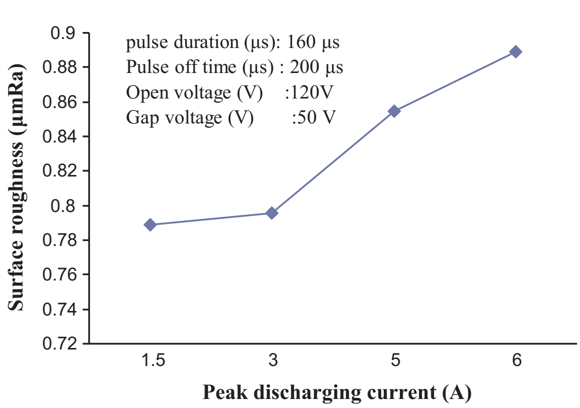

Fig. 6. The relationship between the peak discharging current and surface roughness.

3.2. Cell performance evaluation

In this study, the metallic unipolar plates with flow channels of varying surface roughness were tested for cell performance using the surveying instrument TEI-P300-1AB2CS. Fig. 8 shows the finished SUS316L unipolar plates with the three-pass serpentine flow structure. During tests, this study assembled a single cell 50 mm × 50 mm × 23 mm in dimension, as shown in Fig. 9(a). The cell was fabricated with end plates, gaskets, unipolar plates, and membrane electrode assembly (MEA), as shown in Fig. 9(b). Table 3 shows the cell specifications. The MEA comprised a proton exchange membrane (PEM) and two gas diffusion electrodes (GDE) with 0.25 $mg\,cm^{-2}$ Pt for both the anode and cathode. Pure hydrogen and oxygen were supplied to the anode and cathode electrodes with a flow rate of 60 $cc\,min^{-1}$ and a pressure of 1 atm at room temperature.

Although this study evaluates the performance of unipolar plates by assembling and testing a single cell, the process provided in Section 2 can be applied to fabricate bipolar plates, though the plate thickness is doubled, and the computer-aided coordinate-digitizing system is required to position the flow channels on both sides of the bipolar plates. Applying such bipolar plates to fuel cell stacks increases the thickness of each additional cell merely by less than 2.3 mm (comprising a bipolar plate and an MEA surrounded by two gaskets).

Fig. 10 shows the comparison of cell performances with micro-flow channels of varying surface roughness. As shown in figure, the metallic cell with a surface roughness of 0.715 µm Ra had a maximum power density of 673.5 $mW\,cm^{-2}$. The maximum

Table 3
Cell specifications.

Part	Specification
PEM	DuPont NRE212 Dimension: 30 mm × 30 mm × 0.05 mm
GDE	E-TEK E-LAT® Pt 0.25 $mg\,cm^{-2}$ Dimension: 23 mm × 23 mm × 0.3 mm
Metallic unipolar plate	Stainless steel SUS316L Dimension: 50 mm × 50 mm × 1 mm
Gasket	PTFE film Dimension: 50 mm × 50 mm × 0.15 mm
End plate	Aluminum Dimension: 50 mm × 50 mm × 10 mm

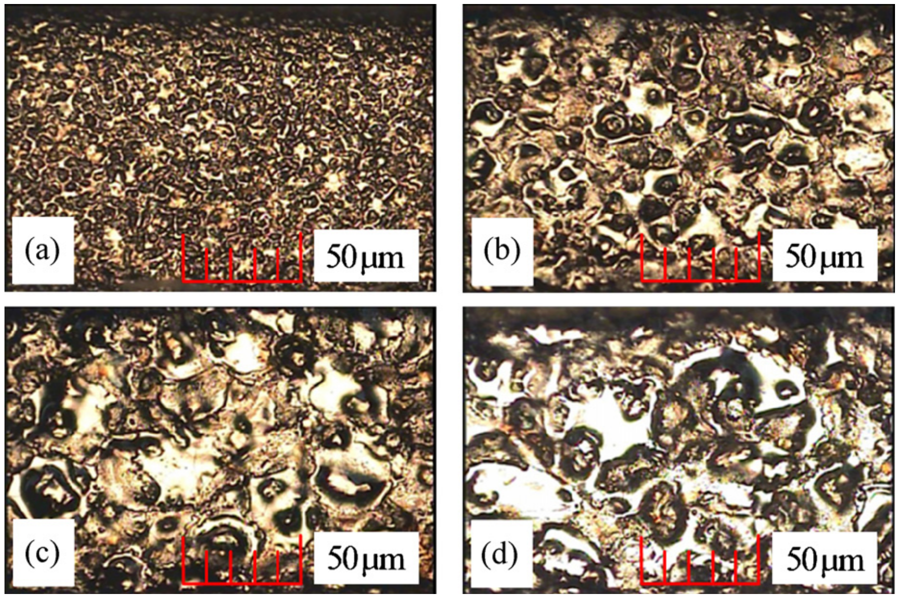

Fig. 7. The surface roughness caused by various peak currents: (a) 1.5 A (0.715 μm Ra), (b) 3 A (0.796 μm Ra), (c) 5 A (0.855 μm Ra), and (d) 6 A (0.994 μm Ra).

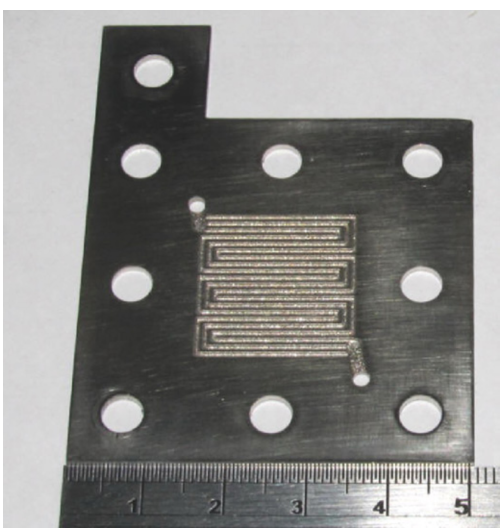

Fig. 8. The SUS316L unipolar plates.

power density of metallic cells with a surface roughness of 0.994 μm Ra reached 646.2 mW cm^{-2}. The volumetric power densities are estimated to be 293 mW cm^{-3} and 281 mW cm^{-3} for a surface roughness of 0.715 μm Ra and 0.994 μm Ra, respectively. The results indicate that cell performance can be slightly improved by lowering the surface roughness of the micro-flow channels, but the magnitude of the improvement may not be statistically significant. The operating parameters that yield the maximum material-removal rate are thus recommended. A previous study based on simulation [21] claimed that the relative roughness height (the ratio of surface roughness to channel depth, r/H) significantly influences the water accumulation. During our experiments, the r/H values were 0.12% and 0.17% for smooth and rough cases, respectively. There was visually no water accumulation in both cases. However, the effect of r/H values on cell performance has not been explored from either modeling or experimental perspectives. With the r/H values in such a small amount in this study, the results indicate that a larger depth might reduce the effect of the surface roughness on cell performance.

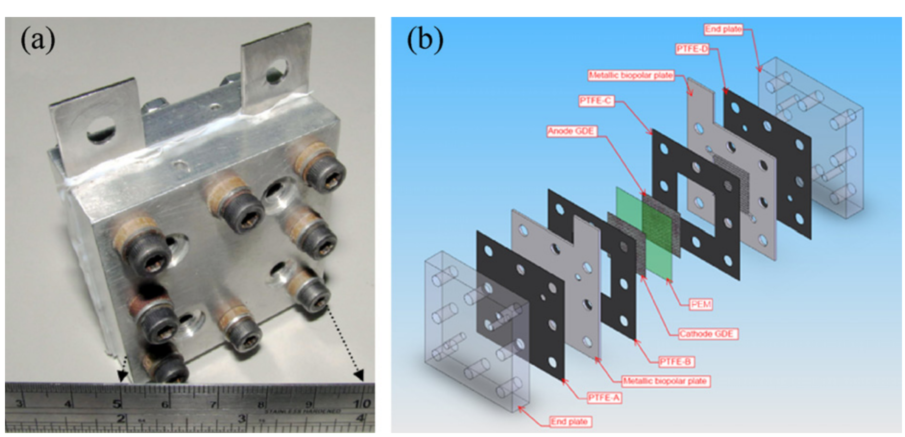

Fig. 9. (a) The assembled cell, and (b) the schematic representation of cell assembly.

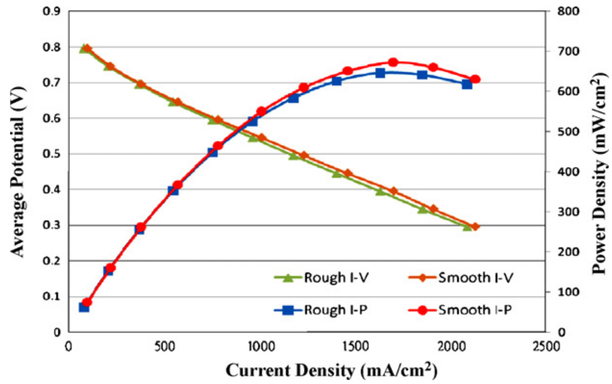

Fig. 10. Comparison of fuel cell performances with flow channels of varying surface roughness.

4. Conclusions

A die-sinking micro-EDM with electrodes prepared using micro-HSM was employed to grow high-aspect-ratio micro-flow channel structures on SUS316L stainless steel plates. The three-pass serpentine with six U-turns was applied as the flow design, of which both the rib and channel widths were 500 μm and the channel depth was 600 μm (aspect ratio = 1.2) in a reaction area of 20 mm $\times$ 20 mm. The high mechanical strength and good electric conductivity of the metallic bipolar plates minimize the size of fuel cells. The experiment result showed that the die-sinking micro-EDM tremendously accelerated the processing time with the material-removal rate as high as 7.2 $mm^3\,min^{-1}$, resulting from a high discharging current, which increases the roughness of channel surfaces. For smoother surfaces (0.715 μm Ra), the maximum power density was 673.5 $mW\,cm^{-2}$; and for coarser surface (0.994 μm Ra) the maximum power density was 646.2 $mW\,cm^{-2}$. Therefore, the effect of surface roughness on cell performance was not obvious in our experiment, probably due to the deep channel depth.

Acknowledgements

The authors would like to thank the National Science Council of Taiwan, R.O.C., for the grant: NSC 99-2622-E-167-009-CC3, which enabled the investigation. The support from Metal Industries Research and Development Centre (MIRDC), who kindly provided Micro-high speed milling equipment, is also greatly appreciated.

References

[1] A. Hermann, T. Chaudhuri, P. Spagnol, International Journal of Hydrogen Energy 30 (2005) 1297–1302.
[2] T. Matsuura, M. Kato, M. Hori, Journal of Power Sources 161 (2006) 74–78.
[3] K. Muammer, S. Mahabunphachai, Journal of Power Sources 172 (2007) 725–733.
[4] R. Hahn, S. Wagner, A. Schmitz, H. Reichl, Journal of Power Sources 131 (2004) 73–78.
[5] N. Kuriyama, T. Kubota, D. Okamura, T. Suzuki, J. Sasahara, Journal of Power Sources 145-146 (2008) 354–362.
[6] J.P. Meyers, H.L. Maynard, Journal of Power Sources 109 (2002) 76–88.
[7] Y. Zhang, J. Lu, S. Shimano, H. Zhou, R. Maeda, Electrochemistry Communications 9 (2007) 1365–1368.
[8] J. Yu, P. Cheng, Z. Ma, B. Yi, Journal of Power Sources 124 (2003) 40–46.
[9] B.Y. Park, M.J. Madou, Journal of Power Sources 162 (2006) 369–379.
[10] D.P. Davies, P.L. Adcock, M. Turpin, S.J. Rowen, Journal of Power Sources 86 (2000) 237–242.
[11] H. Wang, M.A. Sweikart, J.A. Turner, Journal of Power Sources 115 (2003) 243–251.
[12] Y. Wang, L. Pham, G.P.S.D. Vasconcellos, M. Madou, Journal of Power Sources 195 (2010) 4796–4803.
[13] J. Wind, R. Späh, W. Kaiser, G. Böhm, Journal of Power Sources 105 (2002) 256–260.
[14] S.-J. Lee, J.-J. Lai, C.-H. Huang, Journal of Power Sources 145 (2005) 362–368.
[15] S.-J. Lee, C.-Y. Lee, K.-T. Yang, F.-H. Kuan, P.-H. Lai, Journal of Power Sources 185 (2008) 1115–1121.
[16] S.-J. Lee, Y.-M. Lee, C.-Y. Lee, J.-J. Lai, F.-H. Kuan, C.-W. Chuang, Journal of Power Sources 171 (2007) 148–154.
[17] K.P. Rajurkar, G. Levy, A. Malshe, M.M. Sundaram, J. McGeough, X. Hu, R. Resnick, A. DeSilva, CIRP Annals - Manufacturing Technology 55 (2006) 643–666.
[18] J.-C. Hung, T.-C. Yang, K.-C. Li, Journal of Power Sources 196 (2011) 2070–2074.
[19] A.S. Aricò, P. Cretì, V. Baglio, E. Modica, V. Antonucci, Journal of Power Sources 91 (2000) 202–209.
[20] K. Tüber, A. Oedegaard, M. Hermann, C. Hebling, Journal of Power Sources 131 (2004) 175–181.
[21] G. He, Y. Yamazaki, A. Abudula, Journal of Power Sources 195 (2010) 1561–1568.